The Assignment of Generalized Time Constant for A Non-All-Pole System

Yue Qiao, *Student Member, IEEE*, Chengbin Ma, *Member, IEEE*

***Abstract*—This paper discusses the assignment of generalized time constant for a non-all-pole system. The generalized time constant is found to be important because it simultaneously influences the speed of response, damping (i.e. overshoot) and robustness. For the ease of explanation, a general two-mass system is introduced as a case study, which has one pair of $j\omega$-axis zeroes. Under an ideal two-parameter control configuration, the exact lower bound of the generalized time constant is determined that results in monotonic step responses, while a moderate generalized time constant is shown to be desirable for robustness purpose. A m-IPD (modified-Integral-Proportional-Derivative) control configuration is then adopted for the implementation of the ideal two-parameter controller. It is found that in real applications, a specific control configuration and signal delay may also impose limits on the assignment of the generalized time constant and characteristic ratios. Thanks to the clear physical meaning of the polynomial method, the tradeoff relationship among the speed of response, damping and robustness can be explicitly represented. This unique advantage leads to a straightforward controller design procedure. Finally, the theoretical analysis is validated by experimental results.**

***Index Terms*—Polynomial method, non-all-pole system, assignment of generalized time constant, transient response, robustness analysis.**

I. Introduction

In most cases, time response is the final evaluation of the performance of a control system. However, few research directly deals with the control of time response. There is a continuing interest in designing controllers that result in time responses with pre-specified characteristics. Besides classical and modern control, an alternative approach called algebraic design uses polynomial expressions, namely polynomial method. In the method, controllers are designed via the assignment of so-called characteristic ratios and generalized time constant. Both the parameters have clear physical meanings in time response. It was reported that characteristic ratios have a strong relationship with the damping (i.e. overshoot) of a closed-loop system, while the speed of response relates to generalized time constant [1], [2]. Unlike the trial-and-error-based design techniques in classical control, transient responses can be explicitly addressed in polynomial method. In its design procedure, control configuration is defined at the beginning, and then controller parameters are determined under a specific assignment of characteristic ratios and generalized time constant. Therefore, polynomial method is suitable for low-order controller design. It is well-known that the low-order controllers such as the PID-based controllers are predominant in industry. Further improvements on the low-order controller design using the polynomial method would be both theoretically and practically important.

Kessler started the polynomial method and recommended that all the characteristic ratios should be two [3]. Naslin empirically observed the relationships between the characteristic ratios and the transient responses in 1960s [4]. An important contribution is attributed to Manabe, who proposed the Coefficient Diagram Method (CDM) based on Naslin's findings and the Lipatov-Sokolov stability criterion [5]. Using the CDM method, he designed controllers for many successful industrial applications [6], [7]. Characteristic ratio assignment has been empirically discussed and applied in the low-order controller design for a two-mass system [8]. Recently the polynomial method has been extended to new applications such as the force control of a flexible robot system [9], the design of a fractional order controller and its sensitivity analysis [10], [11]. However, the most existing research only emphasized the importance of characteristic ratio assignment. For ideal all-pole systems, it is true that overshoot and the speed of response can be independently controlled, i.e. the shape of the time response is solely determined by characteristic ratios [2]. On the other hand, for the control of more general non-all-pole systems with zeros, overshoot and response speed may not be independently specifiable [2], [12], [13]. Due to the complexity of pole-zero interaction, limits on the assignment of both characteristic ratios and generalized time constant need to be systematically studied. To the authors' knowledge, there is a lack of publications that discuss the assignment of the generalized time constant considering the pole-zero interaction.

Thus this paper deals with polynomial-method-based controller design for a non-all-pole system with zeros, particularly the limits on the assignment of the generalized time constant. The generalized time constant is shown to be important since it simultaneously influences the speed of response, overshoot and robustness. In this paper, ideal general all-pole systems are first discussed including the characteristic ratio assignment and frequency response scaling by the generalized time constant.

Manuscript received April 28, 2013; revised July 22, 2014 and September 30; accepted December 16, 2014. This work was supported by the National Science Foundation of China under Grant 51375299 (2014-2017) and Grant 50905113 (2010-2012).

Copyright (c) 2014 IEEE. Personal use of this material is permitted. However, permission to use this material for any other purposes must be obtained from the IEEE by sending a request to pubs-permissions@ieee.org.

Y. Qiao is with the University of Michigan-Shanghai Jiao Tong University Joint Institute, Shanghai Jiao Tong University, Shanghai 200240, China (e-mail: chimmy@sjtu.edu.cn)

C. Ma is with the University of Michigan-Shanghai Jiao Tong University Joint Institute, Shanghai Jiao Tong University, Shanghai 200240, China; and also with the School of Mechanical Engineering, Shanghai Jiao Tong University, Shanghai, China (e-mail: chbma@sjtu.edu.cn)

In order to facilitate the discussion on non-all-pole systems, break frequencies for the asymptotic bode plot of the closed-loop frequency responses are also accurately calculated. Then a general two-mass system is introduced as a case study. The two-mass system has one pair of $j\omega$-axis zeroes that makes its controller design challenging. With an ideal two-parameter control configuration, the lower bound of the generalized time constant is determined that results in monotonic step responses, while a moderate generalized time constant is shown to be desirable for robustness purpose. A m-IPD (modified-Integral-Proportional-Derivative) control configuration is then introduced for the implementation of the ideal two-parameter controller. It is found a specific control configuration may also impose limits on the assignment of the characteristic ratios and the generalized time constant. Thanks to the clear physical meaning of the polynomial-method-based controller design, the classical tradeoff relationship among the speed of response, damping (i.e., overshoot) and robustness can be explicitly represented. This unique advantage leads to a straightforward controller design procedure. Finally, the theoretical analysis is validated by experimental results.

II. General All-pole Systems

For an initial discussion, a general all-pole closed-loop system with the following transfer function $G(s)$ is first analyzed,

$$G(s) = \frac{a_0}{a_n s^n + a_{n-1}s^{n-1} + ... + a_1 s + a_0}, \tag{1}$$

where a_i $(i = 0, \ldots, n)$ are the coefficients of the characteristic polynomial,

$$P(s) = a_n s^n + a_{n-1}s^{n-1} + ... + a_1 s + a_0. \tag{2}$$

The characteristic polynomial $P(s)$ can be rewritten as a polynomial of a_0, characteristic ratios γ_i (i=1,...,n-1), and generalized time constant τ

$$P(s) = a_0 \left[\frac{1}{\gamma_{n-1}\gamma_{n-2}^2 \cdots \gamma_1^{n-1}} (\tau s)^n + ... + \frac{1}{\gamma_1}(\tau s)^2 + (\tau s) + 1 \right] \tag{3}$$

where γ_i's and τ are defined as

$$\gamma_1 = \frac{a_1^2}{a_0 a_2},\ \gamma_2 = \frac{a_2^2}{a_3 a_1}, \ldots, \gamma_{n-1} = \frac{a_{n-1}^2}{a_{n-2} a_n}, \tag{4}$$

and

$$\tau = \frac{a_1}{a_0}, \tag{5}$$

respectively. Note different with the classical time constant, the generalized time constant τ here is a dimensionless quantity [2]. It is straightforward from the Laplace transform of time-scaled functions that the time response of the all-pole closed-loop system is scaled by the value of the generalized time constant, while the shape of the time response is determined by the characteristic ratios. In addition, the lower-index characteristic ratios, especially γ_1, γ_2, and γ_3, have a more dominant influence [5], [14], [15]. It is known that the standard form of the CDM method, i.e., the Manabe form,

$$\gamma_1 = 2.5 \text{ and } \gamma_i = 2 \text{ for } i = 2, ..., n-1, \tag{6}$$

gives small or non-overshooting step responses, and thus a good starting point for controller design [see Fig. 1] [2], [5], [16]. This form is explained in detail in Appendix A.

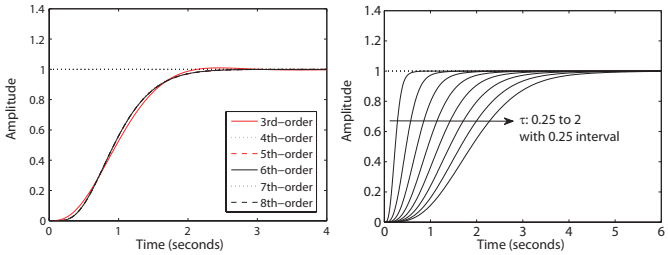

(a) (b)

Fig. 1. Step responses of the general all-pole closed-loop systems under the Manabe form in Equ. (6). (a) Systems of the 3rd to 8th orders and an identical τ(=1 s). (b) A representative case, the 5th-order system with an increasing τ from 0.25 to 2.

Similarly, the frequency response $G(j\omega)$ of the all-pole closed-loop system is

$$G(j\omega) = \frac{1}{\frac{1}{\gamma_{n-1}\gamma_{n-2}^2 \cdots \gamma_1^{n-1}} j^n (\tau\omega)^n + ... + \frac{1}{\gamma_1} j^2 (\tau\omega)^2 + j(\tau\omega) + 1}, \tag{7}$$

which is also scaled by the generalized time constant τ. Under a specific characteristic ratio assignment, the bandwidth of the general all-pole system and τ are inversely proportional. An advantage of the polynomial method is that the characteristic ratios and the generalized time constant have clear physical meanings both in time domain and frequency domain.

In order to facilitate the following analysis of pole-zero interaction, it is convenient to know break frequencies of $G(j\omega)$ at which the slopes are with the unit of -20 dB/decade. While the break frequencies can be approximately determined, the accuracy is problematic due to the complex roots of the characteristic equations under the Manabe form [14]. Considering the generality of the Manabe form, it is worthy to determine the exact frequencies. The break frequencies can be accurately calculated by first solving the following equations,

$$\frac{d\ 20log_{10}|G(j\omega)|}{d\ log_{10}\omega} = -20k \text{ dB/decade, for } k = 1, 2, \ldots, \tag{8}$$

and then finding the intersects of the tangent lines whose slopes are in the unit of -20 dB/decade. The dominant break frequencies, ω_{p0}^*, ω_{p1}^* and ω_{p2}^*, under the Manabe form and a unity τ(=1 s) are listed in Table I. The break frequencies ω_{pi}'s for an arbitrary τ are then scaled by τ as follows

$$\omega_{pi} = \frac{\omega_{pi}^*}{\tau} \text{ for } i = 0, \ldots, n-1. \tag{9}$$

III. Non-all-pole Two-Mass System

For non-all-pole systems, the limitations imposed by zeros have to be addressed. Due to the variety of types of zeros, for ease of explanation, the control of a general two-mass system is discussed as a case study. Many electric drive systems in industry can be modeled as a two-mass system. This benchmark problem is challenging because the two-mass

TABLE I
BREAK FREQUENCIES UNDER MANABE FORM AND A UNITY τ

Order of System	ω_{p0}^*	ω_{p1}^*	ω_{p2}^*
3	1.3473	2.4506	-
4	1.4503	3.1494	4.2755
5	1.4264	3.2855	5.3539
6	1.4251	3.2436	5.4105
7	1.4252	3.2428	5.3668
8	1.4252	3.2429	5.3667

model has one pair of $j\omega$-axis zeroes. Generally, its controller design falls into a category of control problems treated by modern control theory, which usually leads to complicated high-order controllers with difficulties in weighting function selection, parameter tuning, etc [17]–[20]. Intelligent control and fractional order control have also been applied in the two-mass control [21]–[26]. On the other hand, the low-order controllers such as PID-based controllers are predominant in industry. Improvements on low-order controller design would be both theoretically and practically important.

A. Laboratory Torsion System

A torsion test bench is shown in Fig. 2(a) that emulates the two-mass system. With minimized gear backlash, its dynamics is usually simplified as two masses being connected with a non-stiff coupling shaft [see Fig. 2(b)] [8], [27]. Here the dynamics of the gears is treated as a modeling error. Due to the complex gear dynamics, especially with hysteretic and nonlinear gear backlash, this modeling error serves as an effective criterion to judge robustness of the controller design in the following experiments, section V [28]. In the nominal two-mass model, K_s is the spring coefficient. J_m and J_l are the inertias of the drive and load sides, respectively. T_m is driving torque and T_l is disturbance torque. ω_m and ω_l are the velocities of the drive and load sides, respectively.

The transfer function $P(s)$ between driving torque T_m and angular velocity of the drive side ω_m is derived as

$$P(s) = \frac{N(s)}{D(s)} = \frac{s^2 + \omega_a^2}{J_m s(s^2 + \omega_r^2)}, \tag{10}$$

where $N(s)$ and $D(s)$ are the numerator and denominator of $P(s)$. ω_r and ω_a are the natural torsional frequency (NTF) and anti-resonant frequency (ARF),

$$\omega_r = \sqrt{K_s \left(\frac{1}{J_m} + \frac{1}{J_l} \right)} \text{ and } \omega_a = \sqrt{\frac{K_s}{J_l}}, \tag{11}$$

respectively, i.e., the two-mass system has one pair of $j\omega$-axis zeroes,

$$z_{1,2} = \pm j\omega_a. \tag{12}$$

As shown in Table II, the drive and load inertias for the emulated two-mass system can be calculated as

$$J_m = J_{m0} + J_{m1} + (J_{m2} + mJ_{m3})/N_g^2, \tag{13}$$

$$J_l = (J_{l0} + nJ_{l1})/N_g^2, \tag{14}$$

where J_{mi} (i=0,...,3), J_{l0}, and J_{l1} are the inertias of the components. m and n are the numbers of flywheels on the drive and load sides, respectively. N_g(=2) represents the gear ratio, 1:2. There are 2 drive flywheels (m=2) and 5 load flywheels (n=5). The spring coefficient, K_s, of the shaft is measured by the ratio of an applied torque to the angular displacement in experiments. The parameters for the emulated two-mass system in this paper are listed in Table III. Note here the two-mass system serves as an example of a non-all-pole system to facilitate the theoretical discussion on the assignment of generalized time constant. The following approach itself is a general one. It could be applicable to a variety of plants. Meanwhile, various limitations exist in real applications such as nonlinearities including motor torque saturation, gear backlash, signal and plant delays [8], [29]. These nonlinearities may limit the achievable performance of a control system.

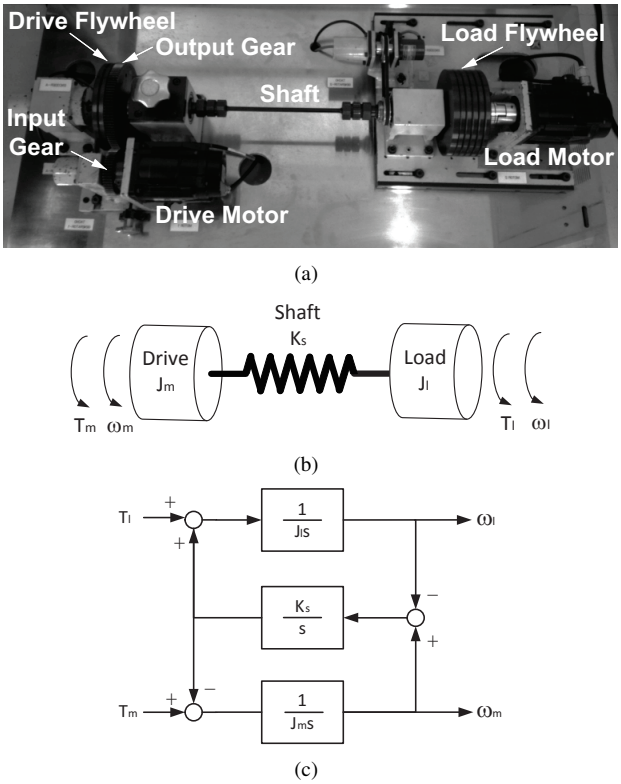

Fig. 2. Torsion test bench and its simplified two-mass model. (a) Test bench. (b) Nominal model. (c) Block diagram.

TABLE II
INERTIAS OF FLYWHEELS AND MOTORS ON DRIVE AND LOAD SIDES

Drive servomotor J_{m0}	3.33×10^{-4} kg · m^2
Drive input gear J_{m1}	5.02×10^{-4} kg · m^2
Drive output gear J_{m2}	6.13×10^{-3} kg · m^2
Drive flywheel J_{m3}	3.66×10^{-3} kg · m^2 (each)
Load side basic J_{l0}	4.29×10^{-3} kg · m^2 (including load servomotor)
Load flywheel J_{l1}	3.79×10^{-3} kg · m^2 (each)

TABLE III
PARAMETERS FOR THE LABORATORY TWO-MASS SYSTEM

J_m(kg · m^2)	J_l(kg · m^2)	K_s(N · m/rad)	ω_a(Hz)	ω_r(Hz)
4.20×10^{-3}	5.81×10^{-3}	39.2	13.1	20.2

B. Transient response

A general two-parameter control configuration is first adopted, as shown in Fig. 3. ω_{ref} is the reference velocity command. For a theoretical discussion, the two controllers $\frac{1}{L(s)}$ and $K(s)$ are specified as

$$\frac{1}{L(s)} = \frac{1}{l_2 s^2 + l_1 s + l_0} \tag{15}$$

$$K(s) = k_2 s^2 + k_1 s + 1, \tag{16}$$

respectively. l_0, l_1, l_2, k_1, k_2 are the coefficients of the controllers. This two-parameter controller is able to independently assign characteristic ratios and generalized time constant, and it does not introduce additional zeroes to the closed loop.

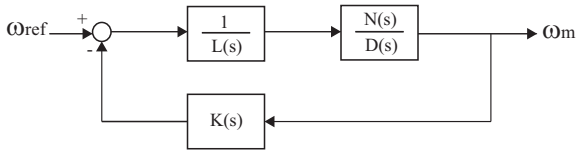

Fig. 3. General two-parameter control configuration

The closed-loop transfer function $M(s)$ of the two-parameter control is

$$M(s) = \frac{N_m(s)}{D_m(s)} = \frac{s^2 + \omega_a^2}{a_5 s^5 + a_4 s^4 + a_3 s^3 + a_2 s^2 + a_1 s + a_0}, \tag{17}$$

where the coefficients a_i $(i = 0, \ldots, 5)$ are

$$a_5 = J_m l_2 = \frac{1}{\gamma_4 \gamma_3^2 \gamma_2^3 \gamma_1^4} \tau^5 a_0 \tag{18}$$

$$a_4 = J_m l_1 + k_2 = \frac{1}{\gamma_3 \gamma_2^2 \gamma_1^3} \tau^4 a_0 \tag{19}$$

$$a_3 = \omega_r^2 J_m l_2 + J_m l_0 + k_1 = \frac{1}{\gamma_2 \gamma_1^2} \tau^3 a_0 \tag{20}$$

$$a_2 = \omega_r^2 J_m l_1 + \omega_a^2 k_2 + 1 = \frac{1}{\gamma_1} \tau^2 a_0 \tag{21}$$

$$a_1 = \omega_r^2 J_m l_0 + \omega_a^2 k_1 = \tau a_0 \tag{22}$$

$$a_0 = \omega_a^2, \tag{23}$$

respectively. $N_m(s)$ and $D_m(s)$ are the numerator and denominator of $M(s)$. The relationship between the characteristic polynomial coefficients and the controller parameters can be described as

$$\begin{bmatrix} a_5 \\ a_4 \\ a_3 \\ a_2 - 1 \\ a_1 \end{bmatrix} = \begin{bmatrix} J_m & 0 & 0 & 0 & 0 \\ 0 & J_m & 0 & 1 & 0 \\ \omega_r^2 J_m & 0 & J_m & 0 & 1 \\ 0 & \omega_r^2 J_m & 0 & \omega_a^2 & 0 \\ 0 & 0 & \omega_r^2 J_m & 0 & \omega_a^2 \end{bmatrix} \cdot \begin{bmatrix} l_2 \\ l_1 \\ l_0 \\ k_2 \\ k_1 \end{bmatrix}. \tag{24}$$

Under a specific assignment of the characteristic ratios γ_i's and the generalized time constant τ, the controller parameters can be uniquely determined by solving the nonhomogeneous matrix equations.

Again, for a smooth transient response, it is desirable that the closed-loop system $M(s)$ has monotonically decreasing magnitude in frequency domain. As illustrated by the Bode plot asymptotes in Fig. 4, by scaling $D_m^*(j\omega)$ whose generalized time constant τ is unity (one), the break frequency of ω_{p1} for the denominator $D_m(j\omega)$ is equal to or smaller than ω_a, the break frequency for the numerator $N_m(j\omega)$ if

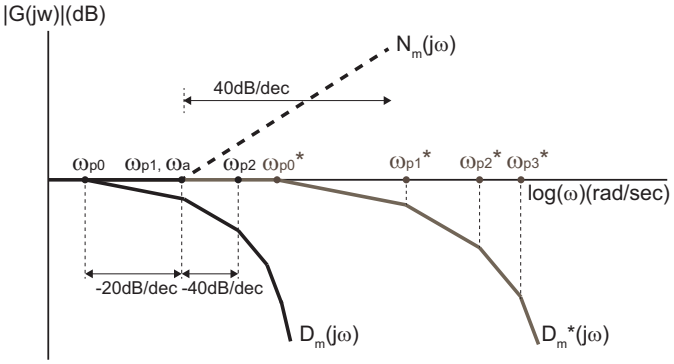

Fig. 4. Frequency response scaling of $D_m(j\omega)$ by τ

$$\tau \geq \tau_c, \tag{25}$$

where the critical τ_c is defined as

$$\tau_c = \frac{\omega_{p1}^*}{\omega_a} \approx 0.0400 \text{ s}. \tag{26}$$

ω_{p1}^* is the exact break frequency for the -40 dB/decade slope of $D_m^*(j\omega)$ under the Manabe form and a unity τ [refer to Table I]. At the frequencies higher than ω_a that corresponds the two zeroes, $\pm j\omega_a$, the decrease in $|D_m(j\omega)|$ is always faster than the increase in $|N_m(j\omega)|$, i.e. the resonant peak of the closed-loop transfer function $M(s)$ can be avoided. Similar consideration using the τ-based scaling of the frequency response is also valid for other non-all-pole systems. As shown in Fig. 5(a), with τ's equal to or greater than 0.0400 s, monotonic step responses can be guaranteed. Compared to the trial-and-error-based sweeping of τ discussed in [16], here the critical τ_c can be accurately determined.

It is known that jω-axis zeroes place a lower bound on the achievable settling time of a closed-loop system that does not lead to excessive overshoot/undershoot, i.e. the limitation on the speed of response [12]. Thanks to the clear physical meaning of the generalized time constant, it is straightforward to design controllers that result in small overshoot for the non-all-pole system.

C. Robustness

The zeroes also limit the robustness performance. The complementary sensitivity function $T(s)$ of the general two-parameter control is

$$T(s) = \frac{K(s)(s^2 + \omega_a^2)}{a_5 s^5 + a_4 s^4 + a_3 s^3 + a_2 s^2 + a_1 s + a_0} = K(s) M(s), \tag{27}$$

where the coefficients a_i's are as same as the coefficients of the closed-loop characteristic equation in Equ. (17). Compared with the closed-loop transfer function $M(s)$, an additional term $K(s)$ appears that relates to robustness. The Bode magnitude plots of $M(s)$ and $K(s)$ with an increasing τ are shown

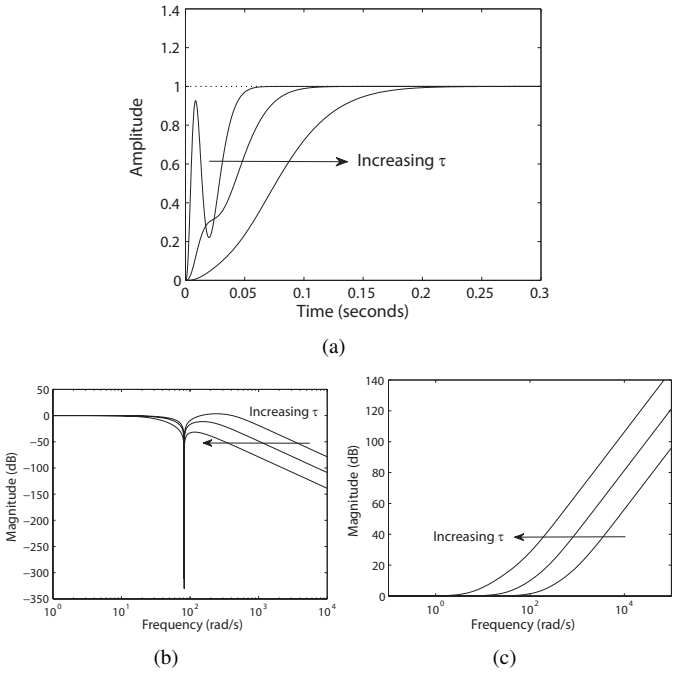

Fig. 5. Time and frequency responses with τ increasing from $\tau_c/2$ to τ_c and $2\tau_c$. (a) Step responses. (b) Closed-loop Bode magnitude plots. (c) Bode magnitude plots of $K(s)$.

in Fig. 5(b) and (c), respectively. As illustrated in Fig. 6, a general conclusion is that, a small τ (i.e. a fast time response) requires a high cutoff frequency of the high-pass term $K(s)$ and slow attenuation of the closed-loop frequency response, thus it tends to cause large peak of $T(s)$ at high frequencies. Similarly, an excessive large τ leads to large peak of $T(s)$ at low frequencies. Namely, the robustness requirement further limits the assignment of the generalized time constant τ. In real applications, a moderate τ needs to be determined under a specific robustness requirement.

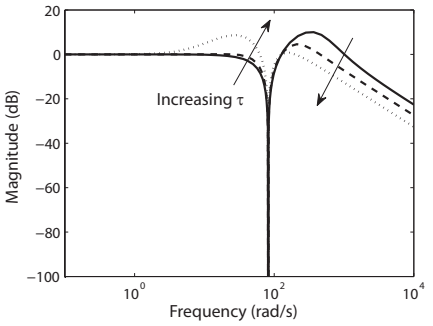

Fig. 6. Bode magnitude plots of the complementary sensitivity functions.

D. Implementation of controller

For the implementation of the two-parameter controller, the block diagram in Fig. 3 can be equivalently transformed to the following one:

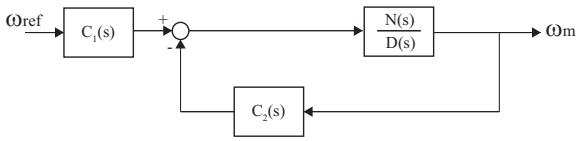

Fig. 7. Equivalent transform of the general two-parameter configuration

where the two controllers $C_1(s)$ and $C_2(s)$ are

$$C_1(s) = \frac{1}{L(s)} = \frac{1}{l_2 s^2 + l_1 s + l_0} \tag{28}$$

$$C_2(s) = \frac{K(s)}{L(s)} = \frac{k_2 s^2 + k_1 s + 1}{l_2 s^2 + l_1 s + l_0}, \tag{29}$$

respectively.

However, for the case study, the control of the two-mass system, disturbance rejection is also required. In the ideal two-parameter control, the transfer function between the disturbance torque T_l and drive velocity ω_m is

$$\frac{\Omega_m(s)}{T_l(s)} = \frac{K_s l_2 s^2 + K_s l_1 s + K_s l_0}{b_5 s^5 + b_4 s^4 + b_3 s^3 + b_2 s^2 + b_1 s + K_s}, \tag{30}$$

where the coefficients b_i $(i = 1, \ldots, 5)$ are

$$b_5 = J_l J_m l_2 \tag{31}$$

$$b_4 = J_l k_2 + J_l J_m l_1 \tag{32}$$

$$b_3 = J_l k_1 + J_l J_m k_0 + J_l K_s l_2 + J_m K_s l_2 \tag{33}$$

$$b_2 = J_l + K_s k_2 + J_l K_s l_1 + J_m K_s l_1 \tag{34}$$

$$b_1 = K_s k_1 + J_l K_s l_0 + J_m K_s l_0. \tag{35}$$

Obviously, with a nonzero l_0 its steady-state response due to a step disturbance torque is also nonzero.

IV. An Alternative Control Configuration

An alternative controller could be the m-IPD (modified-Integral-Proportional-Derivative) controller, a special PID controller using setpoint-on-I-only configuration is applied to approximate the general two-parameter controller, as shown in Fig. 8(a) [8], [30]. The m-IPD control configuration is adopted because it does not introduce any additional zero into the closed-loop transfer function [refer to Equ. (36)]. The so-called IPD controller and its modifications are widely used in servo industry since the discontinuity of the reference command can be smoothed by the integral (i.e. the I controller). As shown in Fig. 8(b)(c), the m-IPD controller is actually equivalent with a special two-parameter controller, which has four unknown controller parameters, K_p, K_i, K_d and T_d. In addition, the m-IPD control has a zero steady-state response due to the step disturbance torque because the corresponding term of l_0 in the m-IPD controller is zero [refer to Equ. (30)]. Note the m-IPD control configuration is a generalization of the configurations of IP, IPD, m-IP, and m-IPD [8].

In [8], the m-IPD controller is designed under the Manabe form, γ_1=2.5, γ_2=2, γ_3=2 and γ_4=2, and thus a fixed generalized time constant too. It is well-known that there is a tradeoff relationship between damping (i.e. overshoot) and robustness in the control of two-mass systems. The standard form emphasizes the damping performance. However, the robustness

problem also needs to be discussed due to the existence of the $j\omega$-axis zeros. A large negative K_d is calculated under the standard form, which leads to a very poor robustness of the control system. As analyzed above, the generalized time constant τ relates to robustness. Thus the m-IPD controller design is further discussed and improved as follows with a more flexible assignment of τ and characteristic ratios.

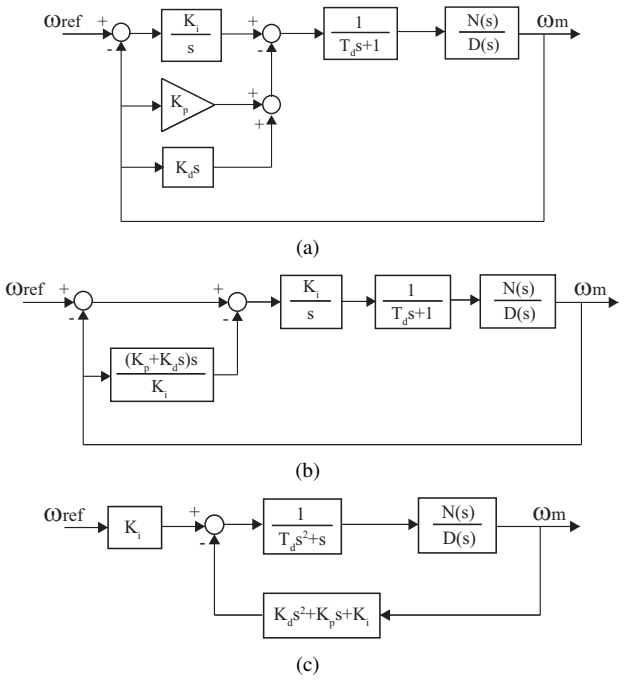

Fig. 8. The block diagram of m-IPD control and its equivalent transforms

For the m-IPD control, its closed-loop transfer function is

$$M^{'}(s) = \frac{K_i(s^2+\omega_a^2)}{a_5^{'}s^5 + a_4^{'}s^4 + a_3^{'}s^3 + a_2^{'}s^2 + a_1^{'}s + a_0^{'}}. \quad (36)$$

Here the coefficients $a_i^{'}$ $(i = 0, \ldots, 5)$ are defined as

$$a_5^{'} = J_m T_d = \frac{1}{\gamma_4\gamma_3^2\gamma_2^3\gamma_1^4}\tau^5 a_0^{'} \quad (37)$$

$$a_4^{'} = J_m + K_d = \frac{1}{\gamma_3\gamma_2^2\gamma_1^3}\tau^4 a_0^{'} \quad (38)$$

$$a_3^{'} = \omega_r^2 J_m T_d + K_p = \frac{1}{\gamma_2\gamma_1^2}\tau^3 a_0^{'} \quad (39)$$

$$a_2^{'} = \omega_r^2 J_m + \omega_a^2 K_d + K_i = \frac{1}{\gamma_1}\tau^2 a_0^{'} \quad (40)$$

$$a_1^{'} = \omega_a^2 K_p = \tau a_0^{'} \quad (41)$$

$$a_0^{'} = \omega_a^2 K_i. \quad (42)$$

Similarly,

$$\begin{bmatrix} a_5^{'} \\ a_4^{'} - J_m \\ a_3^{'} \\ a_2^{'} - \omega_r^2 J_m \\ a_1^{'} \\ a_0^{'} \end{bmatrix} = \begin{bmatrix} J_m & 0 & 0 & 0 \\ 0 & 1 & 0 & 0 \\ \omega_r^2 J_m & 0 & 1 & 0 \\ 0 & \omega_a^2 & 0 & 1 \\ 0 & 0 & \omega_a^2 & 0 \\ 0 & 0 & 0 & \omega_a^2 \end{bmatrix} \cdot \begin{bmatrix} T_d \\ K_d \\ K_p \\ K_i \end{bmatrix}. \quad (43)$$

The nonhomogeneous matrix equations have a unique solution provided that both the ranks of the coefficient matrix and the augmented matrix are as equal as four, i.e., the number of the unknown parameters. Therefore, $a_i^{'}$'s must satisfy the following relationships,

$$a_0^{'} = \omega_a^2(a_2^{'} - \omega_a^2 a_4^{'}) - \omega_a^2(\omega_r^2 - \omega_a^2)J_m, \quad (44)$$

and

$$a_1^{'} = \omega_a^2 a_3^{'} - \omega_a^2\omega_r^2 a_5^{'}. \quad (45)$$

Combined with Eqs. (37)-(42), it can be found

$$a_0^{'} = \frac{\omega_a^2(\omega_r^2 - \omega_a^2)J_m}{\frac{\omega_a^2}{\gamma_1}\tau^2 - \frac{\omega_a^4}{\gamma_3\gamma_2^2\gamma_1^3}\tau^4 - 1} \quad (46)$$

and

$$\frac{\omega_a^2\omega_r^2}{\gamma_4\gamma_3^2\gamma_2^3\gamma_1^4}(\tau^2)^2 - \frac{\omega_a^2}{\gamma_2\gamma_1^2}(\tau^2) + 1 = 0. \quad (47)$$

As shown in Equ. (47), a specific control configuration may also limit the assignment of the characteristic ratios γ_i's and the generalized time constant τ. For the m-IPD control, γ_i's and τ can not be independently specified. Since γ_1, γ_2 and γ_3 are predominant, τ can be determined by specifying γ_4 while letting $\gamma_1 = 2.5$, $\gamma_2 = 2$ and $\gamma_3 = 2$, respectively [refer to Equ. (6)].

For the m-IPD control configuration, the requirement on the damping performance, namely the condition of $\gamma_1 = 2.5$, $\gamma_2 = 2$ and $\gamma_3 = 2$, limits the range of the assignment of the generalized time constant. First in order to have a positive a_0 (i.e. a positive K_i), from Equ. (46) the upper and lower bounds of τ, τ_{max} and τ_{min}, can be derived as

$$\tau_{max,min} = \frac{\gamma_1\gamma_2}{\omega_a}\sqrt{\frac{1 \pm \sqrt{1 - \frac{4}{\gamma_3\gamma_2^2\gamma_1}}}{2}\gamma_3} \quad (48)$$

respectively, namely

$$\tau \in (0.0198 \text{ s},\ 0.0838 \text{ s}), \quad (49)$$

while for real and positive solutions of τ^2 in Equ. (47), the following limit on γ_4 must be satisfied

$$\gamma_4 \geq \frac{1}{2}\left(\frac{\omega_r}{\omega_a}\right)^2 \approx 1.1917, \quad (50)$$

and the lower bound of τ in Equ. (49) is further restricted to a minimum value

$$\tau_{min} = \lim_{\gamma_4 \to \infty} \tau = \frac{\gamma_1}{\omega_a}\sqrt{\gamma_2} \approx 0.0431 \text{ s}. \quad (51)$$

Therefore the upper and lower bounds of τ are finalized as

$$\tau \in [0.0431 \text{ s},\ 0.0838 \text{ s}). \quad (52)$$

Since all the feasible τ's are larger than the critical τ_c (=0.0400 s), monotonic step responses can be guaranteed [see Table IV and Fig. 9]. Note the above available range of τ is under the specific conditions here, i.e., the m-IPD control configuration and the assignment of the characteristic ratios, γ_1=2.5, γ_2=2, and γ_3=2.

As shown in Fig. 10, it is interesting to notice that, thanks to the clear physical meaning of the polynomial method, the

TABLE IV
M-IPD CONTROLLER PARAMETERS

τ (s)	γ_4	K_p	K_i	K_d	T_d
0.0431	88.3892	0.6126	14.2133	-0.0015	0.0000
0.0481	1.8633	0.5721	11.8942	-0.0008	0.0021
0.0531	1.3213	0.5603	10.5520	0.0003	0.0043
0.0581	1.2030	0.5751	9.8983	0.0019	0.0070
0.0631	1.1976	0.6229	9.8718	0.0043	0.0106
0.0681	1.2422	0.7253	10.6506	0.0082	0.0162
0.0731	1.3158	0.9497	12.9913	0.0158	0.0265
0.0781	1.4093	1.6077	20.5852	0.0372	0.0546
0.0831	1.5183	12.6036	151.6680	0.3864	0.5094
0.0837	1.5323	155.9856	1863.6273	4.9364	6.4292

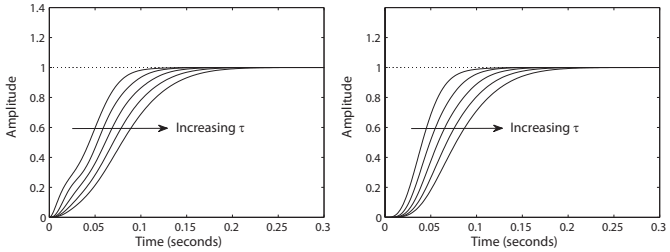

Fig. 9. Monotonic step responses under the m-IPD control with an increasing τ from 0.0431 s, 0.0531 s, 0.0631 s, 0.0731 s to 0.0837 s. (a) Drive velocity ω_m. (b). Load velocity ω_l.

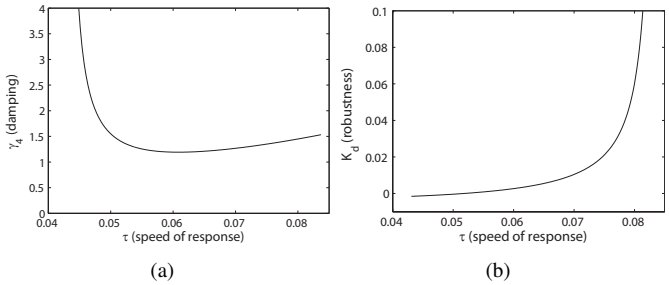

Fig. 10. Interaction among the speed of response, damping and robustness. (a) τ versus γ_4. (b) τ versus K_d.

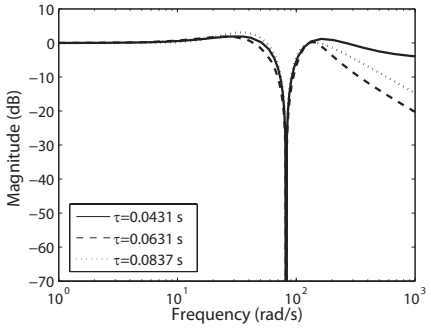

Fig. 11. Bode magnitude plots of the complementary sensitivity functions for the m-IPD control with various τ.

tradeoff relationship among the speed of response, damping (i.e. overshoot) and robustness can be explicitly represented by the interaction among τ, γ_4 and K_d. Similar to the previous theoretical analysis, the robustness of the m-IPD control is largely determined by the high-pass term $(K_d s^2 + K_p s + K_i)$. And under fixed γ_1, γ_2 and γ_3, damping is represented by the value of γ_4. As shown in Table IV and Fig. 10, a small τ leads to a large negative K_d, namely strong positive feedback of the derivative signal and thus a poor robustness, while a large τ corresponds a large positive K_d, which is also not favorable to robustness. Again for the purpose of robustness, a moderate τ is desirable. The complementary sensitivity function $T^{'}(s)$ for the m-IPD can be derived as [refer to Fig. 8(c)]

$$T^{'}(s) = \frac{(K_d s^2 + K_p s + K_i)P(s)}{(T_d s^2 + s) + (K_d s^2 + K_p s + K_i)P(s)}, \qquad (53)$$

where $P(s)$ is the transfer function of the two-mass model described in Equ. (10). The magnitude plots of the complementary sensitivity function with various τ in Fig. 11 validate the above analysis.

Besides, the signal delay may need to be taken into account in the above design of a practical m-IPD controller, especially when the NTF is high (i.e., a high-dynamic drive system). When implementing the controller, the delay occurs during sampling, calculation, and motor torque control. This further limits the assignment of the generalized time constant and the characteristic ratios. PID tuning rules for time-delay systems, such as the Chien-Hrones-Reswick (CHR) settings, can be utilized to provide a reference for determining the parameters [29], [31]. Note in [29] the damping factor ξ relates to the assignment of the characteristic ratios and the controller time constant T_I(=K_p/K_i) is equal with the generalized time constant τ defined here [refer to Eqs. (41)(42)]. In the CHR settings, the recommended T_I (i.e., τ) for PI (i.e., K_d=0) and PID controllers are $T_I > 4T$ and $T_I > 2.38T$, respectively [31]. T is the total delay in a real system. The two inequalities are used that allow consideration of limitation due to the resonance, $T_I \geq 0.5/ARF \approx 0.0382$ s for the current example two-mass system [29]. Since the polynomial-method-based controller design here is based on the two-mass model, the resonance has already been considered. Due to the requirement of non-overshooting step responses (i.e., γ_1=2.5, γ_2=2, and γ_3=2) and the limitation imposed by the m-IPD control configuration, the minimum τ(=0.0431 s) is a little bit greater than 0.0382 s, and $\tau_{min} ARF \approx 0.5637$ [refer to Equ. (51)].

V. EXPERIMENTAL RESULTS

In the experimental system, the torsion test bench is controlled by a PC running on realtime operating system $\mathrm{RTLinux}^{\mathrm{TM}}$. The control programs including the position sampling and speed calculation are written in RTLinux C threads that are executed under the sampling time of 0.001 s in following experiments except the ones investigating the influence of the signal delay. The two sets of industrial servo driving systems are used on the drive and load sides, respectively (drivers: Yaskawa SGDV-3R8A01A, motors: Yaskawa SGMGV-05ADA21). The time constants for the torque control loops of the driving systems are 16 μs. The resolutions of position signals from the two motor rotary encoders are 200,000 pulse/rev. A 12-bit AD/DA multi-functional board is used as the I/O interface with 10 μs conversion time per

channel. Again, the system parameters for the emulated two-mass system are summarized in Table III.

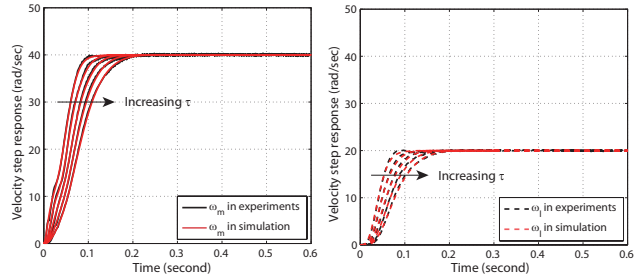

(a) (b)

Fig. 12. Velocity responses with τ from 0.0431 s, 0.0531 s, 0.0631 s, 0.0731 s to 0.0837 s, and minimized gear backlash (black: experiments; red: simulation). (a) the velocity of the drive side, ω_m. (b) the velocity of the load side, ω_l.

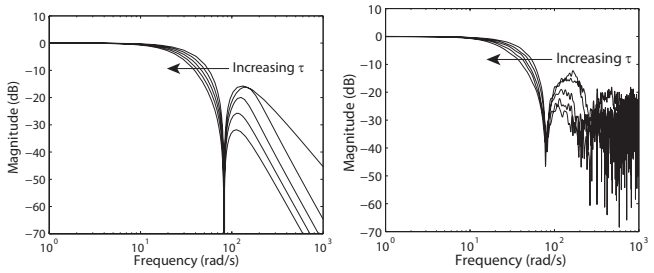

(a) (b)

Fig. 13. Closed-loop frequency responses with τ from 0.0431 s, 0.0531 s, 0.0631 s, 0.0731 s to 0.0837 s, and minimized gear backlash. (a) simulation. (b) experiments.

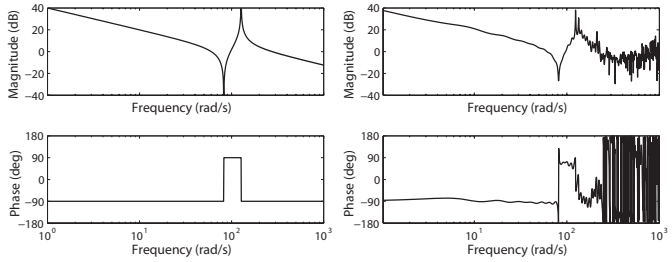

(a) (b)

Fig. 14. Bode plots of the open-loop two-mass system. (a) simulation. (b) experiments.

The actual dynamics of the laboratory torsion system is obviously much more complex than the dynamics described by the ideal two-mass model, particularly due to the existence of gears. On the other hand, this modeling error can be utilized to effectively verify the robustness of the controller design. First the nominal velocity responses with minimized gear backlash are shown in Fig. 12 for the m-IPD control. Due to the gear ratio of 1:2, the drive velocity ω_m is two times faster than the load velocity ω_l. The experimental results (black) well match the simulation results (red). This validates the nominal two-mass model. Consistent with the previous theoretical analysis, the monotonic step responses are observed in all the velocity responses except when τ=0.0431 s, i.e., the smallest τ. The small overshoot in the case (the smallest τ) indicates a deteriorated robustness against gear backlash that is with a high frequency dynamics. The experimental closed-loop frequency responses are extracted from the above step responses, and shown in Fig. 13(b). The high-frequency noises are mainly caused by the complex dynamics of the gears. It can be seen that the frequency responses are scaled by τ. Since all the τ's are larger than the critical τ_c(=0.0400 s), the resonance peak is avoided. For reference purposes, the Bode plots of the open-loop two-mass system for the experimental set-up are also shown in Fig. 14(b) and compared with the nominal ones in Fig. 14(a). The natural torsional and anti-resonant frequencies of the experimental set-up well match their respective nominal values. This good match illustrates the correctness of the parameters determined in Table III, section III-A.

Then a step load disturbance torque (5 N·m from 0.4 s) and relatively large gear backlash ($\pm$0.6 degree) are introduced to further investigate the robustness performance. As shown in Fig. 15, moderate τ's such as 0.0531 s and 0.0631 s are desired. Both the smallest and largest τ's, 0.0431 s and 0.0837 s, show a poor robustness against the gear backlash nonlinearity. In additional, the largest τ(=0.0837 s) leads to slower disturbance rejection performance. This result well verifies the robustness analysis in section III-C.

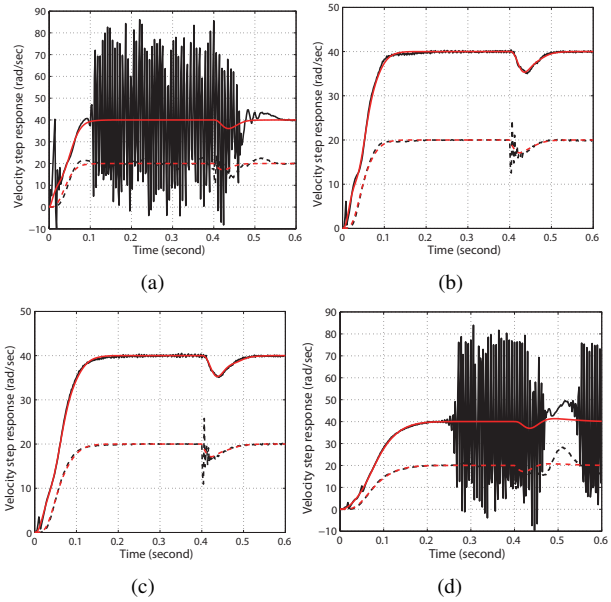

(a) (b) (c) (d)

Fig. 15. Velocity responses with $\pm$ 0.6 deg. gear backlash and 5 N·m load disturbance torque from 0.4 second. (a) τ=0.0431 s. (b) τ=0.0531 s. (c) τ=0.0631 s. (d) τ=0.0837 s.

For comparison purposes, an alternative control method, the slow resonance ratio control, is applied here. This method is from a well-cited reference, [27], for the control of two-mass systems. Besides the IP (Integral-Proportional) controller, a disturbance observer (DOB) is introduced to virtually change the inertia ratio R=KR_0, where K is a constant and R_0 is the real inertia ratio defined as J_l/J_m in the reference. In its design procedure, fixed K_p and K_i are first designed based on the one-mass model $\frac{1}{(J_l+J_m)s}$ and the value of ω_a, the ARF of

the two-mass system; then the parameters of the DOB, K and T_q, are determined in an iterative manner [refer to section III-D and E in [27]]. T_q is the cut-off frequency of the Q-filter in the DOB. The experimental results using the slow resonance ratio control are shown in Fig. 16. Here K is 1.2016 and T_q=0.0075. They are determined to exactly have a same virtual inertia ratio R in the experimental example of [27]. It can be seen that with minimized gear backlash (i.e., close to the ideal two-mass system), the controllers designed by the two methods (polynomial method and slow resonance ratio control) have a comparable performance. However, when the gear backlash is relatively large the system becomes unstable under the current controller design. Note the polynomial method is a general design tool because it is based on the closed-loop transfer functions, and thus not limited to a specific control configuration. Actually, the current design of the IP controller and the DOB in the slow resonance ratio control can be improved using the polynomial method [32]. Besides, the polynomial method is efficient to simultaneously determine all the controller parameters, i.e., K_p, K_i, K, and T_q here.

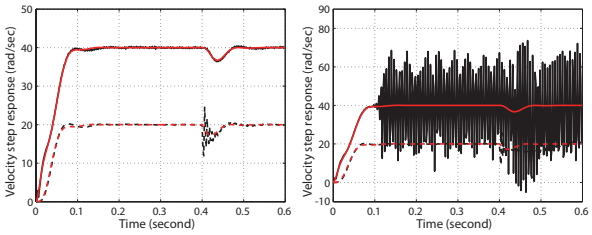

Fig. 16. Velocity responses under the slow resonance ratio control and 5 N·m load disturbance torque from 0.4 second (black: experiments; red: simulation). (a) with minimized gear backlash. (b) with ± 0.6 deg. gear backlash.

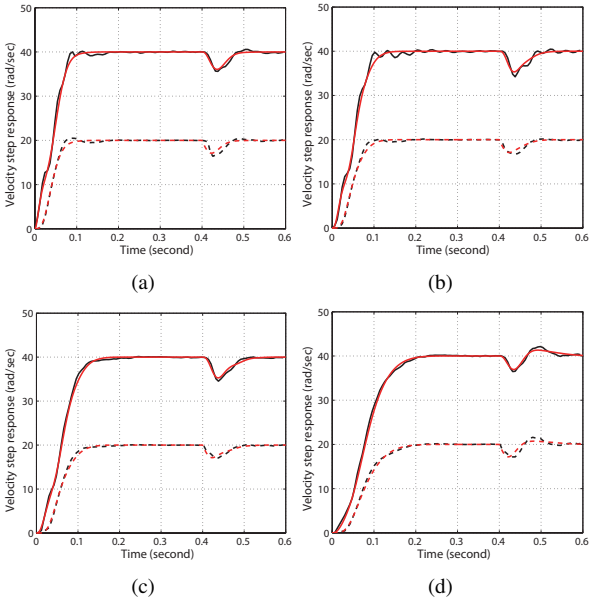

Fig. 17. Velocity responses under 0.003 s sampling time and with minimized gear backlash and 5 N·m load disturbance torque from 0.4 second (black: experiments; red: simulation). (a) τ=0.0431 s. (b) τ=0.0531 s. (c) τ=0.0631 s. (d) τ=0.0837 s.

Finally, in order to investigate the influence of the signal delay, the sampling time is intentionally increased to 0.003 s, three times larger than the sampling time in the previous experiments. The results clearly show that the assignment of the generalized time constant (i.e., the speed of response) is further limited by the signal delay, especially for the application in high-dynamic drive systems [29]. For a smooth non-overshooting step response, longer the signal delay, greater the required generalized time constant τ. Again, τ need to be determined considering the influences of both delay and resonance.

VI. Conclusions

This paper discusses the limits on the assignment of the generalized time constant for a non-all-pole system. The requirement of a smooth transient response imposes a lower bound on the assignment of the generalized time constant that avoids a large overshoot. An excessive small or large generalized time constant are both unfavorable in terms of robustness performance. A moderate generalized time constant needs to be determined under a certain robustness requirement. In real applications, a specific control configuration and signal delay may also limit the assignment of the generalized time constant and its interactive relationship with the characteristic ratios. It is shown that the clear physical meaning of the polynomial method leads to a straightforward controller design procedure. This unique advantage would be desirable for industrial applications.

The future works may include applying the polynomial method in the controller design for more complicated and realistic systems. It is also of practical importance to develop a general design scheme for higher-order systems, such as a three-mass system, in which direct equation solving may become too complicated. In addition, extending the polynomial method to the design of multi-input-multi-output (MIMO) control systems would further broaden its applications.

Appendix A
Manabe Form

Non-overshooting step responses are usually of interest in order to establish a guideline for the controller design. It can be proved that for the all-pole system $G(s)$ in Equ. (1), it has monotonically decreasing magnitude in frequency response, and thus small overshoot in step response under the condition that all the characteristic ratios are larger than two [2]. In addition, the lower-index characteristic ratios, particularly γ_1, γ_2 and γ_3 have a more dominant influence [5], [14], [15]. Therefore, overshoot can be adjusted using a single characteristic ratio γ_1 with all the other higher-index characteristic ratios fixed at two. This specific characteristic ratio assignment can be defined as

$$\gamma_1 = \gamma_1^* \text{ and } \gamma_i = 2 \text{ for } i = 2, ..., n-1, \qquad (54)$$

where γ_1^*'s are the minimum values of γ_1 that enable non-overshooting step responses. Due to the well-known difficulty in finding exact analytical solutions for systems of order higher than two, γ_1^*'s listed in Table V are determined numerically

by searching γ_1^* while letting all the other higher-index characteristic ratios be fixed at two. As shown in Table V, it is interesting to notice that despite the different orders of the systems, all the γ_1^*'s are close to 2.5. This characteristic ratio assignment is actually identical to the so-called standard form of the CDM method, i.e., the Manabe form here, which was based on intensive experimental studies [refer to Equ. (6)] [2], [5], [16].

TABLE V
MINIMUM γ_1 FOR NON-OVERSHOOTING STEP RESPONSES

System Order	3	4	5	6	7	8
γ_1^*	2.61	2.53	2.48	2.48	2.48	2.48

REFERENCES

[1] Y. C. Kim, L. H. Keel, and S. Manabe, "Controller design for time domain specifications," in *Proc. IFAC The 15th Triennial World Congress*, Barcelona, Spain, 2002.

[2] Y. C. Kim, L. H. Keel, and S. P. Bhattacharyya, "Transient response control via characteristic ratio assignment," *IEEE Trans. Autom. Control*, vol. 48, no. 12, pp. 2238–2244, 2003.

[3] V. C. Kessler, "Ein beitrag zur theorie mehrschleifiger regelungen," *Regelungstechnik*, vol. 8, no. 8, pp. 261–266, 1960.

[4] P. Naslin, *Essentials of optimal control*. Iliffe, 1968.

[5] S. Manabe, "Importance of coefficient diagram in polynomial method," in *Proc. 42nd IEEE Annual Conference on Decision and Control*, vol. 4, 2003, pp. 3489–3494.

[6] ——, "Controller design of two-mass resonant system by coefficient diagram method," *Transactions-Institute of Electrical Engineers of Japan D*, vol. 118, no. 1, pp. 58–66, 1998.

[7] K. S. R. Hirokawa and S. Manabe, "Autopilot design for a missile with reaction-jet using coefficient diagram method," in *Proc. AIAA Guidance, Navigation, and Control Conference*, Montreal, Canada, 2001, pp. 1–8.

[8] C. Ma, J. Cao, and Y. Qiao, "Polynomial method based design of low-order controllers for two-mass system," *IEEE Trans. Ind. Electron.*, vol. 60, no. 3, pp. 969–978, 2013.

[9] C. Mitsantisuk, M. Nandayapa, K. Ohishi, and S. Katsura, "Resonance ratio control based on coefficient diagram method for force control of flexible robot system," in *Proc. 12th IEEE International Workshop on Advanced Motion Control*, 2012, pp. 1–6.

[10] M. Tabatabaei and M. Haeri, "Characteristic ratio assignment in fractional order systems," *ISA transactions*, vol. 49, no. 4, pp. 470–478, 2010.

[11] ——, "Sensitivity analysis of CRA based controllers in fractional order systems," *Signal Processing*, vol. 92, no. 9, pp. 2040–2055, 2012.

[12] G. C. Goodwin, A. R. Woodyatt, R. H. Middleton, and J. Shim, "Fundamental limitations due to jω-axis zeros in SISO systems," *Automatica*, vol. 35, no. 5, pp. 857–863, 1999.

[13] J. Stewart and D. E. Davison, "On overshoot and nonminimum phase zeros," *IEEE Trans. Autom. Control*, vol. 51, no. 8, pp. 1378–1382, 2006.

[14] Y. C. Kim, K. H. Lee, and Y. T. Woo, "A note on bode plot asymptotes based on transfer function coefficients," in *Proc. International Conference on Control, Automation and Systems*, Gyeong Gi, Korea, 2005, pp. 664–669.

[15] Y. C. Kim, K. Kim, and S. Manabe, "Sensitivity of time response to characteristic ratios," *IEICE Transactions on Fundamentals of Electronics, Communications and Computer Sciences*, vol. 89, no. 2, pp. 520–527, 2006.

[16] L. Keel, Y. Kim, and S. Bhattacharyya, "Advances in three term control," in *Pre-congress tutorials & workshops, 17th IFAC World Congress*, Seoul, Korea, 2008.

[17] R. Dhaouadi, K. Kubo, and M. Tobise, "Two-degree-of-freedom robust speed controller for high-performance rolling mill drives," *IEEE Trans. Ind. Appl.*, vol. 29, no. 5, pp. 919–926, 1993.

[18] K. Sugiura and Y. Hori, "Vibration suppression in 2-and 3-mass system based on the feedback of imperfect derivative of the estimated torsional torque," *IEEE Trans. Ind. Electron.*, vol. 43, no. 1, pp. 56–64, 1996.

[19] M. Hirata, K. Z. Liu, and T. Mita, "Active vibration control of a 2-mass system using μ-synthesis with a descriptor form representation," *Control Engineering Practice*, vol. 4, no. 4, pp. 545–552, 1996.

[20] E. Omine, T. Goya, U. Akie, T. Senjyu, A. Yona, N. Urasaki, and T. Funabashi, "Torsional torque suppression of decentralized generators using H∞ observer," *Renewable Energy*, vol. 35, no. 9, pp. 1908–1913, 2010.

[21] L. Wang and Y. Frayman, "A dynamically generated fuzzy neural network and its application to torsional vibration control of tandem cold rolling mill spindles," *Engineering Applications of Artificial Intelligence*, vol. 15, no. 6, pp. 541–550, 2002.

[22] K. B. Lee and F. Blaabjerg, "An improvement of speed control performances of a two-mass system using a universal approximator," *Electrical Engineering*, vol. 89, no. 5, pp. 389–396, 2007.

[23] T. Orlowska-Kowalska and K. Szabat, "Control of the drive system with stiff and elastic couplings using adaptive neuro-fuzzy approach," *IEEE Trans. Ind. Electron.*, vol. 54, no. 1, pp. 228–240, 2007.

[24] ——, "Neural-network application for mechanical variables estimation of a two-mass drive system," *IEEE Trans. Ind. Electron.*, vol. 54, no. 3, pp. 1352–1364, 2007.

[25] T. Orlowska-Kowalska, M. Dybkowski, and K. Szabat, "Adaptive sliding-mode neuro-fuzzy control of the two-mass induction motor drive without mechanical sensors," *IEEE Trans. Ind. Electron.*, vol. 57, no. 2, pp. 553–564, 2010.

[26] K. Erenturk, "Fractional order PI$^\lambda$D$^\mu$ and active disturbance rejection control of nonlinear two mass drive system," *IEEE Trans. Ind. Electron.*, vol. 60, no. 9, pp. 3806–3813, 2013.

[27] Y. Hori, H. Sawada, and Y. Chun, "Slow resonance ratio control for vibration suppression and disturbance rejection in torsional system," *IEEE Trans. Ind. Electron.*, vol. 46, no. 1, pp. 162–168, 1999.

[28] M. Nordin and P.-O. Gutman, "Controlling mechanical systems with backlash - a survey," *Automatica*, vol. 38, no. 10, pp. 1633–1649, 2002.

[29] R. Muszynski and J. Deskur, "Damping of torsional vibrations in high-dynamic industrial drives," *IEEE Trans. Ind. Electron.*, vol. 57, no. 2, pp. 544–552, 2010.

[30] C. T. Chen, *Analog and digital control system design: transfer-function, state-space, and algebraic methods*. New York, USA: Oxford University Press, Inc., 1995.

[31] M. Araki, "PID control," *Control systems, robotics and automation*, vol. 2, pp. 1–23, 2002.

[32] Y. Qiao, L. Zhou, and C. Ma, "Polynomial-based inertia ratio controller design for vibration suppression in two-mass system," in *Industrial Electronics Society, IECON 2013-39th Annual Conference of the IEEE*, Vienna, Austria, Nov. 10-13, 2013, pp. 3687–3692.

Yue Qiao received the B.S.E.E. degree in 2010 and M.S. degree in 2013 both from the University of Michigan-Shanghai Jiao Tong University Joint Institute, Shanghai Jiao Tong University, where he is currently working toward the Ph.D. degree.

His research interests include theory and application of motion control and mechatronics.

Chengbin Ma (M'05) received the B.S.E.E. (Hons.) degree from East China University of Science and Technology, Shanghai, China, in 1997, and the M.S. and Ph.D. degrees both in the electrical engineering from University of Tokyo, Tokyo, Japan, in 2001 and 2004, respectively.

He is currently a tenure-track assistant professor of electrical and computer engineering with the University of Michigan-Shanghai Jiao Tong University Joint Institute, Shanghai Jiao Tong University, Shanghai, China. He is also with a joint faculty appointment in School of Mechanical Engineering, Shanghai Jiao Tong University. Between 2006 and 2008, he held a post-doctoral position with the Department of Mechanical and Aeronautical Engineering, University of California Davis, California, USA. From 2004 to 2006, he was a R&D researcher with Servo Laboratory, Fanuc Limited, Yamanashi, Japan. His research interests include motion control and mechatronics, networked hybrid energy systems, and wireless power transfer.